Proceedings of the 21st ICSMGE, Vienna, Austria, 14 – 19 June 2026. Pistrol, Adam & Schweiger (eds.)
Published by: ÖGG, Austrian Society for Geomechanics, Salzburg, Austria, ISBN 978-3-9503898-4-5
https://doi.org/10.53243/ICSMGE2026-1202

Stability of slurry-supported diaphragm wall corners

Johannes Stamm, Markus Herten
Chair of Geotechnics, University of Wuppertal, Germany, stamm@uni-wuppertal.de

Matthias Pulsfort
Ingenieurgesellschaft für Spezialtiefbau mbH, Wuppertal, Germany

ABSTRACT: In Germany, the stability of slurry-supported diaphragm walls is generally not verified by trial trenches, as is the case abroad, but by calculation. The national standard DIN 4126 'Stability analysis of diaphragm walls' is used for this purpose. Among others, it must be verified that a soil body will not slide into the trench and compress it. Here the unfavourable effect of the earth pressure force is opposed to the favourable effect of the supporting pressure force. The limited length of the trench results in a three-dimensional rather than a plane earth pressure condition. The earth pressure is therefore lower than in the plane case. A pseudo-spatial method is used to calculate the spatial active earth pressure, which reduces the earth pressure by shear stress parallel to the sliding surface on the Coulomb wedge. A practical approach only exists for plane diaphragm wall trenches. In practice, diaphragm walls often have to be designed as corner slots, in T- or L-shapes, and as polygonal elements, e.g. excavation corners. Both the determination of the three-dimensional earth pressure forces and the effective support pressure forces are geometrically more demanding than for a plane trench of limited length. For this reason, a test rig has been designed to investigate the stability failure of a diaphragm wall corner as described above on a model scale. The aim of the investigations is to understand the failure kinematics and to extend the design concept to diaphragm wall corners. Initial investigations have shown that the failure kinematics are highly dependent on the spatial ratio. Since the failure kinematics of the diaphragm wall corner are similar to those of the plane diaphragm wall, the aim is to extend the application of pseudo-spatial calculation method of DIN 4126 to diaphragm wall corners.

KEYWORDS: diaphragm wall corner, slurry-supported, stability analysis, pseudo-spatial earth pressure, analytical approach.

1 INTRODUCTION

Diaphragm walls are a construction method used in specialist foundation engineering. They are not only used as low-deformation, water impermeable excavation pits, but also for example for deep foundations. Thereby vertical loads are transferred via base resistance as well as skin friction and horizontal loads via bedding stresses. Regardless of the application, the essential manufacturing feature is the section-by-section excavation of panels, which are produced using a diaphragm wall grabber or a diaphragm wall hydro mill. The resulting cavity is filled with a support fluid, usually bentonite suspensions, but increasingly also with polymer solutions (Stocker & Walz, 2003).

Both the German standardisation concept (DIN 4126, 2013) and internationally distributed analytical and numerical approaches, which have been verified by corresponding model tests, are available for calculating the stability of fluid-supported diaphragm wall panels. However, these investigations only relate to plane trenches. In almost all applications, however, there are trenches that are snapped off in plan, usually right-angled corners in the form of T- or L-shaped panels. There are far fewer publications on this subject: The problem was first analysed by Triantafyllidis et al. (2001). Here, the stability of non-plane trenches is calculated in a simplified manner by replacing the geometry with a plane trench of modified length. This paper has been revised by Triantafyllidis et al. (2011). In addition, Grandas-Tavera & Triantafyllidis (2012) carried out numerical calculations for soft clayey soils with an anisotropic visco-hypoplastic constitutive law. For such non-plane trenches, there are no corresponding model tests available that could verify the analytical and numerical calculations.

In this paper, Section 2.1 first explains analytical earth pressure approaches used to calculate the stability (Section 2.2) of fluid-supported diaphragm walls. Section 3 then presents a model experimental rig that can be used to analyse the stability of slurry-supported diaphragm wall corners on a model scale. Finally, in Section 4, the earth pressure approach by Triantafyllidis et al. (2001) will be modified based on the test results.

2 FUNDAMENTALS

2.1 *Analytical earth pressure approaches for slurry-supported diaphragm walls*

In practice, in addition to numerical calculation methods, analytical calculation methods have been established in order to calculate the spatial earth pressure on a plane trench. As diaphragm wall panels only have a limited length in relation to their depths, spatial conditions occur for the earth pressure. This is lower than the earth-pressure on an infinitely long wall (Coulomb's theory) due to an arching effect in soil. A distinction is made here between geometric-spatial and pseudo-spatial methods, whereby the former do not play any role in practise due to their application limits.

The pseudo-spatial methods utilise a prismatic earth wedge according to Coulomb, but add sliding surface-parallel shear forces T on the end faces of the wedge, which reduce the earth pressure in comparison to the infinitely long wall. Figure 1 shows the earth pressure approach of DIN 4126 (2013). The focus of the pseudo-spatial methods is not on modelling the failure body to be observed, but on a static concept for the application of the forces. Equilibrium conditions (Σ H and Σ V) at the earth wedge are obtained:

$$E_{\mathrm{agh}}^{\mathrm{r}} = [G - (2T + K) \cdot \sin(\vartheta)] \cdot \tan(\vartheta - \varphi) - (2T + K) \cdot \cos(\vartheta) \quad (1)$$

According to Coulomb's theory, the failure angle ϑ is to be varied to obtain the maximum earth pressure force. To calculate the shear force T, either a stress distribution approach can be specified (Walz & Pulsfort, 1983) or set equal to the vertical stress present inside the earth wedge prism (Walz & Hock, 1987). In both cases, it is important that the vertical stress σ_z increases sublinear with depth due to vertical arching effects. DIN 4126 (2013) uses a bilinear distribution for the vertical stresses.

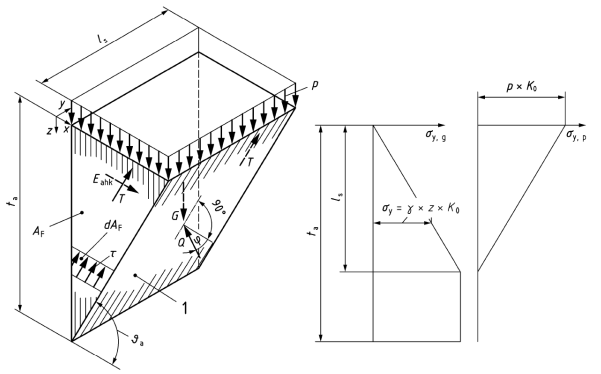

Figure 1. Soil wedge in the earth pressure approach of DIN 4126 (2013)

For non-plane geometries, a pseudo-spatial soil body can also be used, which is extended by an overhang compared to the soil wedge for a plane trench (Triantafyllidis et al., 2001). This results in a higher weight of the soil body with constant shear forces, which leads to an increase in earth pressure force compared to the plane case. The soil body for calculation of the spatial earth pressure on a diaphragm wall corner with legs of equal length is shown in Figure 2.

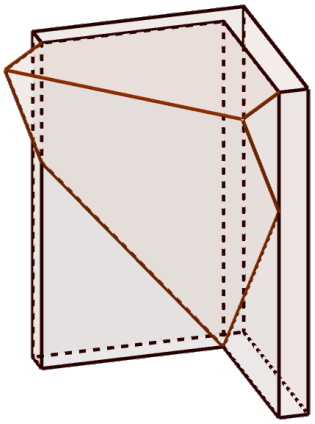

Figure 2. Soil body for calculation of the earth pressure on a slurry-supported corner trench

The geometry of the soil body is to be varied in order to find the form leading to the maximum earth pressure force.

2.2 *Stability considerations*

External stability is the term used to describe the failure of a soil body into the trench, as the hydrostatic force of the support-fluid cannot stabilise the soil body. For stability analysis in accordance with Eurocode 7, the design value of the earth pressure force E_{ah} must therefore be less than the design value of the support force S:

$$E_{ah,d} \leq S_d \tag{2}$$

In Germany, the panel stability is specified more precisely by DIN 4126 (2013) and assigned to the HYD/UPL limit state:

$$\gamma_{G,dst} \cdot E_{ah,k} \leq \gamma_{G,stb} \cdot S_k \tag{3}$$

For the further investigations, the proof equation according to (3) is rewritten as follows, so that a global factor of safety η will be defined as:

$$\eta = S_k / E_{ah,k} \geq \gamma_{G,dst} / \gamma_{G,stb} \tag{4}$$

The support force S_k is calculated by integrating the difference between the hydrostatic pressure of the support fluid and the water pressure (net support pressure) over the contact area between soil body and support fluid. For coarse-grained soils with penetration of the support fluid into the grain structure, the support force is to be reduced (DIN 4126, 2013).

3 MODEL TESTS

3.1 *Theoretical considerations*

A model on a scale of 1:10 was selected for the investigation of the stability of a diaphragm wall corner as illustrated in Figure 3. The trench is produced "as wished" using a perforated plate template. This method has already been tested in model tests for plane trenches next to isolated footings by Pulsfort (1986) and Happe (1996) resulting in a significant time saving compared to production with a model hydro mill (Waldhoff, 1991). Various geometries can be investigated using different perforated plate templates.

In order to obtain information on the failure body geometry and kinematics, the ultimate limit state of the slurry-supported trench must be reached in the model test. This is achieved in the tests by raising the water level or by lowering the support-fluid level respectively. With both methods, this reduces the net support pressure forces, causing a failure. This procedure was first used by Elson (1968).

A narrow-graded medium to coarse sand with a grain size of 0.1 to 1.0 mm was selected as test soil.

3.2 *Test setup*

The experimental rig consists of a sealed box measuring 1.90 m x 0.96 m x 1.00 m. The water level can be adjusted as required via two water chambers, whereby the water level can communicate via a 5 cm thick layer of gravel at the bottom of the test box. In order to achieve filter stability of the gravel layer in relation to the test soil, a commercially available non-woven fabric is installed at the top of the gravel layer. The three-part, stiffened perforated plate template (h = 90 cm) is placed on a support plate and sealed on the outside with a layer of thin paper so that the test soil cannot trickle into the trench. In addition, the paper prevents the bentonite suspension from any penetration into the soil, so that the net support pressure is transferred via a membrane by normal stresses.

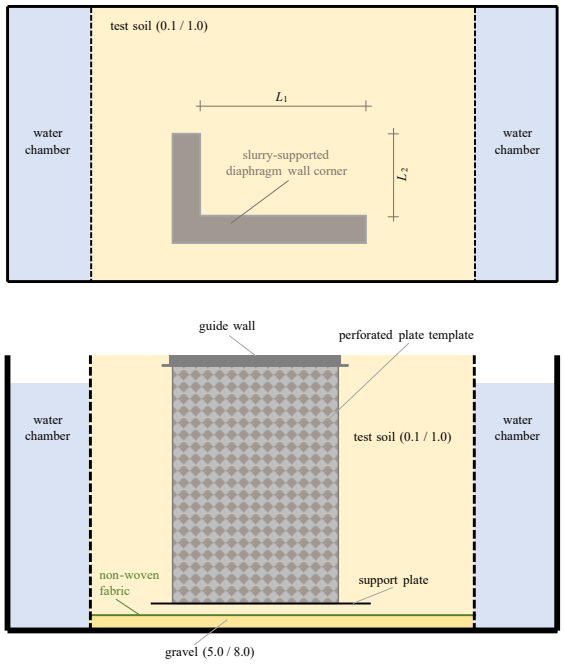

Figure 3. Model (scale 1:10) for the investigation of the panel stability of diaphragm wall corners, above: top view, below: sectional view

In order to identify the failure body, marking layers of white fine-grained sand were trickled every 5 cm. After installation of the test soil, a 4 cm high guide wall made of a stainless-steel angle profile was installed at the top of the trench. Then, the trench template was filled with slurry, using a bentonite concentration of 40 g/ℓ. Now, the earth wall was supported by hydrostatic pressure of the slurry and the perforated plate could be folded inwards and removed.

To reach the limit state, the water level in the rig was then slowly raised. A speed of 0.2 to 0.25 ℓ/s was selected, which corresponds to a rising speed of approx. 1.0 cm/min. Reaching the limit state is defined by sliding of the soil body into the trench. In order to expose the failure body, the trench was concreted with a flowable cement mortar using the tremie method. After setting and hardening of the mortar, the moist test soil could be removed vertically, slice by slice, due to its apparent cohesion. The offset of the marking layers enabled the shear band to be identified.

3.3 *Variation of the installation method of the test soil*

Various installation methods using kinetic energy for compaction were investigated with regard to their relative density and its variation:

- sand rain method
- single grain trickle method
- jet trickle method

With all three methods, the test soil was dropped into the test rig from a defined height. First, the required drop height was determined for each method in a small-scale test by varying the kinetic energy. In addition, the density was measured over the height in the test rig in order to assess the uniformity. The sand rain method and the jet trickle, which were also used in model tests by Pulsfort (1986) or Herten (1999), produced a significantly lower density than the single grain trickle. The difference compared with experiments of Pulsfort (1986) and Herten (1999) lay in the position of the trench, which is not at the edge but in the centre of the test box. This caused higher turbulences within the test rig. The single grain trickle method (Lo Presti et al., 1992), in which sand is scattered from a funnel with a constant drop height not only produced the highest density – very dense according to the density index of ISO 14688-2 (2017) – but also a good reproducibility. Figure 4 shows the distribution of the dry density of the sand over the height. With a coefficient of variation of 0.48 %, the scatter is very low.

3.4 *Test results*

Three different geometries were analysed:

- plane trench with a panel length of 60 cm
- corner trench with inner leg lengths L_1 = 60 cm / L_2 = 30 cm
- corner trench with inner leg lengths L_1 = 60 cm / L_2 = 60 cm

The height of the diaphragm wall corners produced was uniformly 90 cm.

3.4.1 *Plane trench*

A plane trench with a length of 60 cm was carried out as reference test. This resulted in a shell-shaped failure body, which was also observed in tests conducted by Karstedt (1980). The difference between support-fluid level and groundwater level in the ultimate limit state was slightly lower than in Karstedt's tests. This difference can be explained by the guide wall, which absorbs part of the earth pressure (Pulsfort, 1986).

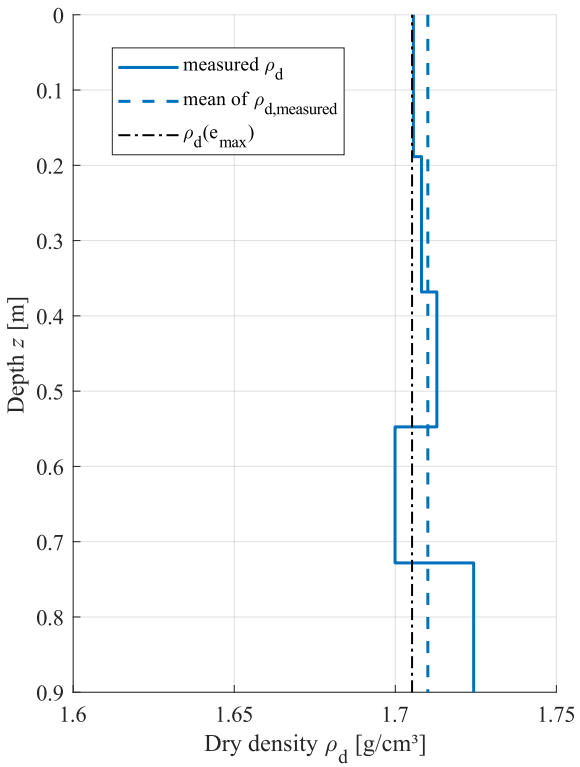

Figure 4. Measured dry density ρ_d in the model test versus depth z and maximum density at e_{max}

3.4.2 *Corner trench 60 / 30*

As could be expected, the 60 / 30 cm corner trench showed a lower stability than the 60 cm long plane trench. The failure body was a convexly curved body at the ground surface, which runs between the two inner leg corners. The stitch of the curvature was approx. 8 cm in relation to the diagonal of the inner leg corners. Figure 5 shows the top view of a test after exceeding the ultimate limit state.

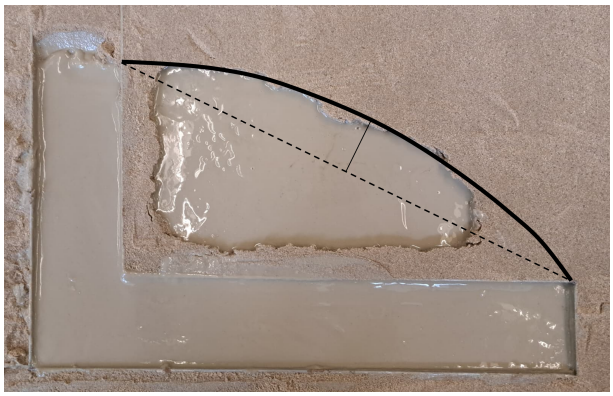

Figure 5. Top view of model test "Corner Trench 60/30" after reaching the ultimate limit state.

The shear band can be clearly recognized along the exposed failure body (Figure 6). It has no strong curvature in the cross section and is very steep (approx. 90°), especially in the upper area. Failure angles of 75° - 80° were measured in the lower area. Figure 7 shows an example of the measured points on the failure surface as a point cloud with an interpolation of the surface. This clearly shows that it is not continuously convex in the lower area. The failure body is aligned along the longer leg of the corner, widening towards the short leg.

Figure 6. Visualisation of the shear band by the offset of the marking layers after exposing the failure body slice by slice

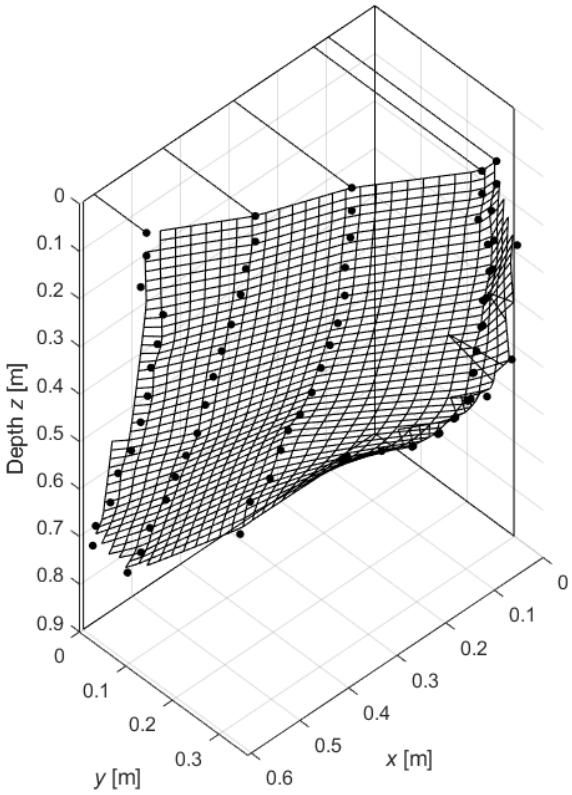

Figure 7. Measured points and interpolation of failure surface of model test "Corner Trench 60 / 30"

3.4.3 *Corner trench 60 / 60*

In the case of an isosceles corner trench (inner leg lengths 60 cm each), two independent failure bodies occurred, which failed in quick succession, each parallel to the adjacent panel leg. Figure 8 shows the primary failure and the secondary failure when the ultimate limit state was exceeded.

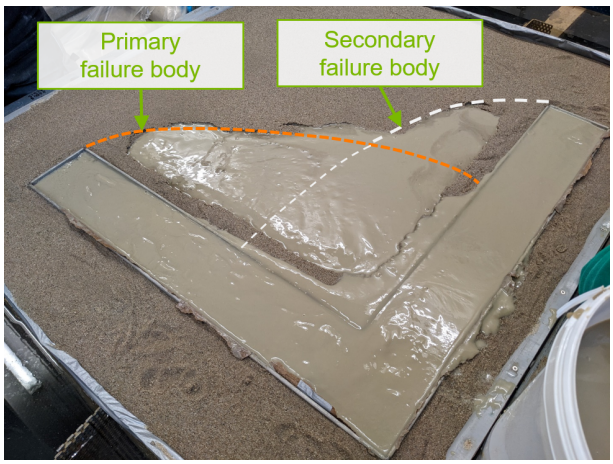

Figure 8. Primary failure and secondary failure of model test "Corner Trench 60 / 60" after exceeding the ultimate limit

3.5 *Summary of model tests*

In the model tests, the shell-like failure body form described in the literature could be confirmed for the plane trench. For the isosceles corner trenches, it was observed that two independent failure bodies occur for both panel legs for the investigated spatial ratio (panel depth H to panel diagonal L at ratio H / L) ≤ 1.06 in the model scale. In the case of the non-isosceles corner, a failure parallel to the longer leg was observed.

The FE simulations of Grandas-Tavera & Triantafyllidis (2012), in which a flat failure surface and a small failure angle at the base the trench with cylindrical, prismatic attachment was found, could not be confirmed in the tests with sand. However, it should be noted that material law used by Grandas-Tavera & Triantafyllidis (2012) represents the deformation behaviour of cohesive, normal to slightly over-consolidated soils. Also, the spatial ratio in the numerical simulations ($H / L \in [4.23; 6.31]$) differs from the model tests presented.

4 MODIFICATION OF THE EXISTING EARTH PRESSURE APPROACH

4.1 *Failure body geometry*

The model test results motivate not only to vary the failure angle ϑ when selecting the geometry of the failure body, but also to orientate the shear plane arbitrarily in space. If a plane, non-kinked failure surface (analogous to the pseudo-spatial failure body of DIN 4126 (2013)) remains unchanged, the orientation angle ψ of the failure body as shown in Figure 9 can be introduced as second degree of freedom of the shear plane.

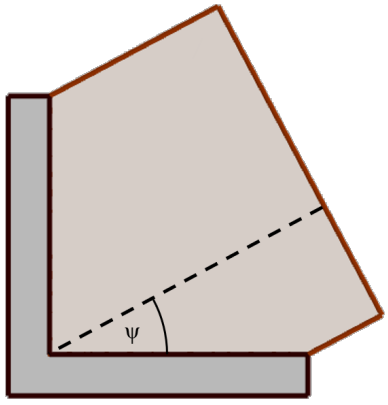

Figure 9. Definition of the second degree of freedom (orientation angle ψ) of the failure body

This corresponds to a possible rotation of the shear plane around the z-axis, where $\psi \in [0°, 90°]$ applies. For the boundary values, this results in the two failure bodies of a plane trench with a reduced area of one of the end faces and thus a lower shear force T. This failure mode is referred to below as parallel failure, as the line of intersection of failure surface with the ground surface is parallel to one of the panel legs. For $\psi = \psi_0$ with

$$\psi_0 = \arctan(L_1 / L_2) \quad (5)$$

the earth pressure approach presented by Triantafyllidis et al. (2001) results.

It is important to recognise that not only the magnitude of the earth pressure force $E_{ah,k}$ depends on ϑ and ψ, but also the magnitude of the support force S_k concerning the equations (3) and (4). The reason is that the significant area over which the net support pressure is integrated is also dependent on ϑ and ψ.

As a result, it is not sufficient to determine the maximum earth pressure force for corner trenches, but rather to maximise the utilisation ratio respectively to find the minimum factor of safety η according to equation (4).

4.2 *Results for corner trench with isosceles panel legs*

For a corner trench with panel leg ratio of 1:1, it is sufficient to consider $\psi \in [0°, 45°]$ for mode symmetry reasons. For shallow excavation depths, parallel failure ($\psi = 0°$) provides the lowest factor of safety. This is due to the fact that the spatial ratio (panel depth H to panel diagonal L) is very low for shallow excavation depths. With increasing depth and the resulting increasing spatial ratio, the failure body orientation ψ shifts from 0° to 45°. Figure 10 shows the factor of safety η according to equation (4) over the depth for different values of ψ. The dimensions of the panel and the soil properties correspond to the example as given by Triantafyllidis et al. (2011):

Dimensions of L-Panel:

$L_1 = L_2 = 6/\sqrt{2} = 4{,}24$ m
$\gamma_{bentonite} = 10{,}5$ kN/m³ $\gamma_{water} = 10{,}0$ kN/m³
bentonite level: $z_F = 0{,}30$ m
guide wall depths $z_g = 1{,}50$ m

Soil properties:

granular soil
$\gamma_{unsat} = 18{,}5$ kN/m³ $\gamma_{sat} = 20{,}0$ kN/m³
$\varphi' = 32{,}5°$ $c' = 0$ kN/m²
groundwater level: $z_w = 2{,}50$ m

As can be seen in Figure 10, the global factor of safety η is very high near the guide wall and then decreases with increasing depth. Instead of the support pressure, the earth pressure at rest in front of the guide wall was used (Pulsfort, 1986) related to the diagonal length of the soil body (Triantafyllidis et al., 2011).

For the given geometry and soil parameters the earth pressure approach of Triantafyllidis et al. (2011) is only relevant for depths greater than 6.00 m, corresponding to a spatial ratio of 1.0. Above this depth, other orientations of the soil body (ψ) have to be considered, too. Those can be decisive, in particular, if there is a soil layer with lower shear strength or a soil layer with high permeability so that the support force is to be reduced due to penetration according to DIN 4126 (2013).

4.3 *Results for corner trench with non-isosceles panel legs*

For a corner trench with non-isosceles panel legs, all orientations $\psi \in [0°, 90°]$ must be considered. As an example, a corner trench with leg length $L_1 = 6{,}00$ m and $L_2 = 4{,}00$ m is regarded. The soil parameters are identical to the example in Section 4.2. Figure 11 shows the factor of safety for different values of ψ dependant on the excavation depths.

In contrast to a corner trench with isosceles panel legs, the orientation ψ does not converge towards ψ_0 for large depths or large spatial ratios.

5 CONCLUSION

In this paper a test rig was presented in which model tests for stability of slurry-supported diaphragm wall corners can be carried out on a scale of 1:10. Raising the water level can cause global stability failure. Various installation methods of the test soil (sand 0.1-1.0 mm) were tested in order to achieve the most homogeneous and reproducible density in the test box. Model tests with 3 different geometries were carried out using the single grain trickle method. The failure bodies were exposed vertically slice by slice and measured.

Depending on the spatial ratio investigated either a parallel failure or a spatial failure could be observed. Therefore, it is recommended to modify the earth pressure approach of Triantafyllidis et al. (2011): An additional degree of freedom (orientation angle ψ) was introduced, so that failure surface can rotate around the z-axis. Stability analyses varying ϑ and ψ with this failure body have shown that the type of failure mode depends on the spatial ratio.

For corner trenches with isosceles panel legs, the earth pressure corresponds to the solution of Triantafyllidis et al. (2011) for a certain depth. For corner trenches with non-isosceles panel legs, other failure body geometries also need to be investigated.

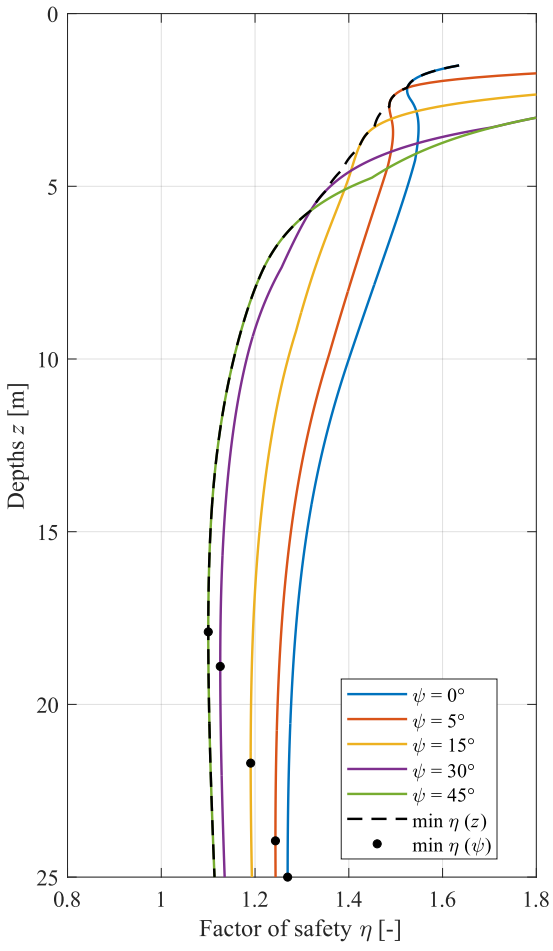

Figure 10. Factor of safety η versus depth for a corner trench with isosceles panel legs ($L_1 = L_2 = 4.24$ m)

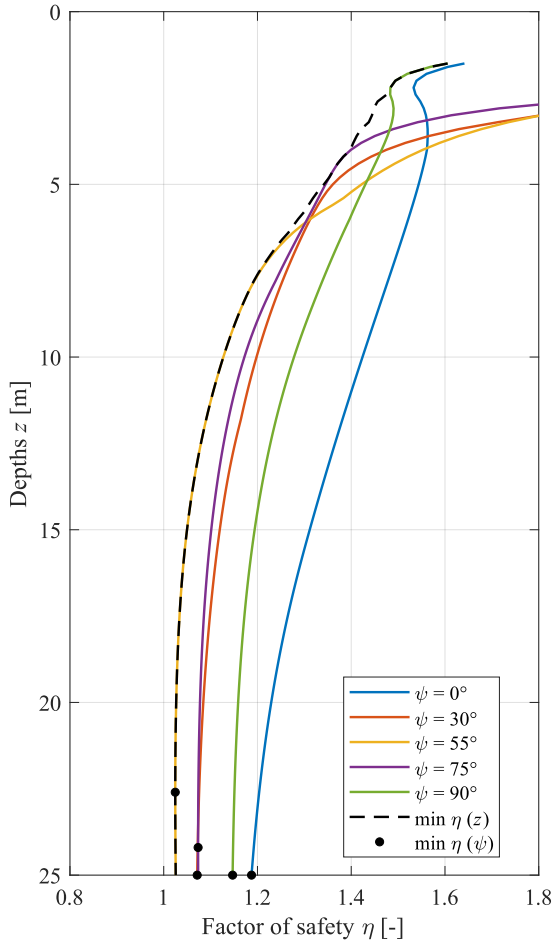

Figure 11. Factor of safety η versus depth for a corner trench with non-isosceles panel legs (L_1 = 6.00 m, L_2 = 4.00 m)

6 LITERATURE

Elson, W. K. 1968. An experimental investigation of the stability of slurry trenches. *Geotechnique* 18(1), 37–49.

Grandas-Tavera, C. E., and Triantafyllidis, T. 2012. Simulation of a corner slurry trench failure in clay. *Computers and Geotechnics* 45, 107–117.

Happe, T. 1996. *Entwicklung eines empirisch-mathematischen Verfahrens zur Abschätzung der Setzungen von Einzelfundamenten neben suspensionsgestützten Schlitzen begrenzter Länge*. Wuppertal: Bergische Universität Gesamthochschule Wuppertal, Fachbereich Bauingenieurwesen.

Herten, M. 1999. *Räumlicher Erddruck auf Schachtbauwerke in Abhängigkeit von der Wandverformung*. Aachen. Shaker Verlag.

Karstedt, J.-P. 1980. *Untersuchungen zum aktiven räumlichen Erddruck im rolligen Boden bei hydrostatischer Stützung der Erdwand.* Berlin: Grundbauinstitut der Technischen Universität Berlin.

Lo Presti, D. C. F., Pedroni, S., and Crippa, V. 1992. Maximum dry density of cohesionless soils by pluviation and by ASTM D 4253-83. A comparative study. *Geotechnical Testing Journal* 15(2), 180–189.

Pulsfort, M. 1986. *Untersuchungen zum Tragverhalten von Einzelfundamenten neben suspensionsgestützten Erdwänden begrenzter Länge.* Wuppertal: Bergische Universität Gesamthochschule Wuppertal, Fachbereich Bautechnik.

Stocker, M., Walz, B. 2003. Bored pile walls, diaphragm walls, cut-off walls. In: Smoltcyk, U. 2003. *Geotechnical Engineering Handbook – Volume 3: Elements and Structures.* Berlin: Ernst & Sohn Verlag.Ch.3.6.

Triantafyllidis, T., König, D., and Sonntag, M. 2001. Zur äußeren Standsicherheit von nicht-ebenen suspensionsgestützten Erdschlitzen. *Bautechnik* 78(2), 77-78.

Triantafyllidis, T., Vogelsang, J., and Grandas-Tavera, C. E. 2011. Zur Standsicherheit suspensionsgestützter Eckschlitzwandelemente. *Bautechnik* 88(9), 617–626.

Waldhoff, P. 1991. *Untersuchungen zum Setzungsverhalten von Einzelfundamenten neben flüssigkeitsgestützten Erdwänden begrenzter Länge*. Wuppertal: Bergische Universität Gesamthochschule Wuppertal, Fachbereich Bautechnik.

Walz, B., and Hock, K. 1987. *Berechnung des räumlichen aktiven Erddrucks mit der modifizierten Elementscheibentheorie.* Wuppertal: Bergische Universität Gesamthochschule Wuppertal, Fachbereich Bautechnik.

Walz, B., and Pulsfort M. 1983. Rechnerische Standsicherheit suspensionsgestützter Erdwände. *Tiefbau, Ingenieurbau, Straßenbau* 25(1,2), 8-12 & 82-86.

Deutsches Institut für Normung, 2013. *DIN 4126 Nachweis der Standsicherheit von Schlitzwänden*. Berlin: DIN.

International Organization for Standardization, 2017. *ISO 14688-2 Geotechnical investigation and testing — Identification and classification of soil — Part 2: Principles for a classification. Genf*, Switzerland: ISO.